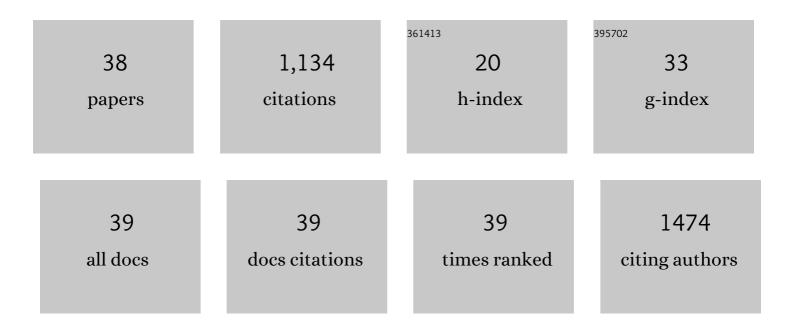


List of Publications by Year in descending order

Source: https://exaly.com/author-pdf/708245/publications.pdf Version: 2024-02-01



\<u>\/fi Xi</u>A

#	Article	IF	CITATIONS
1	Regulation of DNA-binding activity of the Staphylococcus aureus catabolite control protein A by copper (II)-mediated oxidation. Journal of Biological Chemistry, 2022, 298, 101587.	3.4	2
2	Inhibition of SARS-CoV-2 replication by zinc gluconate in combination with hinokitiol. Journal of Inorganic Biochemistry, 2022, 231, 111777.	3.5	10
3	In Situ Prodrug Activation by an Affibodyâ€Ruthenium Catalyst Hybrid for HER2â€Targeted Chemotherapy. Angewandte Chemie, 2022, 134, .	2.0	4
4	In Situ Prodrug Activation by an Affibodyâ€Ruthenium Catalyst Hybrid for HER2â€Targeted Chemotherapy. Angewandte Chemie - International Edition, 2022, 61, .	13.8	24
5	Inhibition of Quorum-Sensing Regulator from Pseudomonas aeruginosa Using a Flavone Derivative. Molecules, 2022, 27, 2439.	3.8	8
6	Identification of an Au(I) N-Heterocyclic Carbene Compound as a Bactericidal Agent Against Pseudomonas aeruginosa. Frontiers in Chemistry, 2022, 10, 895159.	3.6	3
7	Solution structure of a thrombin binding aptamer complex with a non-planar platinum(<scp>ii</scp>) compound. Chemical Science, 2022, 13, 8371-8379.	7.4	5
8	Lightâ€Triggered Nitric Oxide Release by a Photosensitizer to Combat Bacterial Biofilm Infections. Chemistry - A European Journal, 2021, 27, 5453-5460.	3.3	26
9	Allosteric inhibition of SARS-CoV-2 3CL protease by colloidal bismuth subcitrate. Chemical Science, 2021, 12, 14098-14102.	7.4	19
10	Oxidative stress transforms 3CLpro into an insoluble and more active form to promote SARS-CoV-2 replication. Redox Biology, 2021, 48, 102199.	9.0	8
11	Identification of a Novel Inhibitor of Catabolite Control Protein A from <i>Staphylococcus aureus</i> . ACS Infectious Diseases, 2020, 6, 347-354.	3.8	10
12	Structural Insight into the Substrate Gating Mechanism by <i>Staphylococcus aureus</i> Aldehyde Dehydrogenase. CCS Chemistry, 2020, 2, 946-954.	7.8	18
13	Charge-driven tripod somersault on DNA for ratiometric fluorescence imaging of small molecules in the nucleus. Chemical Science, 2019, 10, 10053-10064.	7.4	33
14	Identification and Characterization of a Metalloprotein Involved in Gallium Internalization in <i>Pseudomonas aeruginosa</i> . ACS Infectious Diseases, 2019, 5, 1693-1697.	3.8	16
15	Deciphering molecular mechanism of silver by integrated omic approaches enables enhancing its antimicrobial efficacy in E. coli. PLoS Biology, 2019, 17, e3000292.	5.6	66
16	Combination of gallium(<scp>iii</scp>) with acetate for combating antibiotic resistant <i>Pseudomonas aeruginosa</i> . Chemical Science, 2019, 10, 6099-6106.	7.4	52
17	Inactivation of NikR from Helicobacter pylori by a bismuth drug. Journal of Inorganic Biochemistry, 2019, 196, 110685.	3.5	6
18	The unique trimeric assembly of the virulence factor HtrA from Helicobacter pylori occurs via N-terminal domain swapping. Journal of Biological Chemistry, 2019, 294, 7990-8000.	3.4	16

WEI XIA

#	Article	IF	CITATIONS
19	Multi-omics and temporal dynamics profiling reveal disruption of central metabolism in <i>Helicobacter pylori</i> on bismuth treatment. Chemical Science, 2018, 9, 7488-7497.	7.4	33
20	Conformational equilibria and intrinsic affinities define integrin activation. EMBO Journal, 2017, 36, 629-645.	7.8	112
21	Integrative approach for the analysis of the proteome-wide response to bismuth drugs in Helicobacter pylori. Chemical Science, 2017, 8, 4626-4633.	7.4	66
22	Competition for Iron Between Host and Pathogen: A Structural Case Study on Helicobacter pylori. Methods in Molecular Biology, 2017, 1535, 65-75.	0.9	6
23	Identification of catabolite control protein A from <i>Staphylococcus aureus</i> as a target of silver ions. Chemical Science, 2017, 8, 8061-8066.	7.4	27
24	Bismuth-Induced Inactivation of Ferric Uptake Regulator from <i>Helicobacter pylori</i> . Inorganic Chemistry, 2017, 56, 15041-15048.	4.0	24
25	Targeting the Thioredoxin Reductase–Thioredoxin System from <i>Staphylococcus aureus</i> by Silver Ions. Inorganic Chemistry, 2017, 56, 14823-14830.	4.0	24
26	Relating conformation to function in integrin α ₅ β ₁ . Proceedings of the National Academy of Sciences of the United States of America, 2016, 113, E3872-81.	7.1	110
27	Exploration into the nickel â€~microcosmos' in prokaryotes. Coordination Chemistry Reviews, 2016, 311, 24-37.	18.8	15
28	Metal ion and ligand binding of integrin α ₅ β ₁ . Proceedings of the National Academy of Sciences of the United States of America, 2014, 111, 17863-17868.	7.1	86
29	Functional disruption of HypB, a GTPase of Helicobacter pylori, by bismuth. Chemical Communications, 2014, 50, 1611-1614.	4.1	22
30	Nickel translocation between metallochaperones HypA and UreE in Helicobacter pylori. Metallomics, 2014, 6, 1731-1736.	2.4	34
31	Histidine-rich proteins in prokaryotes: metal homeostasis and environmental habitat-related occurrence. Metallomics, 2013, 5, 1423.	2.4	26
32	Interaction of SlyD with HypB of Helicobacter pylori facilitates nickel trafficking. Metallomics, 2013, 5, 804.	2.4	30
33	Metallo-GTPase HypB from Helicobacter pylori and Its Interaction with Nickel Chaperone Protein HypA. Journal of Biological Chemistry, 2012, 287, 6753-6763.	3.4	50
34	Multifaceted SlyD from Helicobacter pylori: implication in [NiFe] hydrogenase maturation. Journal of Biological Inorganic Chemistry, 2012, 17, 331-343.	2.6	40
35	Solution structure of GSP13 from Bacillus subtilis exhibits an S1 domain related to cold shock proteins. Journal of Biomolecular NMR, 2009, 43, 255-259.	2.8	9
36	Structure of a Nickel Chaperone, HypA, from Helicobacter pylori Reveals Two Distinct Metal Binding Sites. Journal of the American Chemical Society, 2009, 131, 10031-10040.	13.7	90

WEI XIA

#	Article	IF	CITATIONS
37	1H, 13C, and 15N resonance assignments of a general stress protein GSP13 from Bacillus subtilis. Biomolecular NMR Assignments, 2008, 2, 163-165.	0.8	2
38	CHAPTER 14. Nickel Metallochaperones: Structure, Function, and Nickel-Binding Properties. 2-Oxoglutarate-Dependent Oxygenases, 0, , 284-305.	0.8	2